Elastic properties of a confined fluid

J. M. Rickman
Department of Materials Science and Engineering and Department of Physics, Lehigh University, Bethlehem, Pennsylvania 18015, USA
(Received 7 October 2012; published 26 December 2012)

Monte Carlo computer simulation is employed to determine the local, wave-number-dependent, high-frequency elastic properties of a Lennard-Jones fluid that is confined between two walls. In particular, the elastic constants are calculated from coarse-grained stress correlation functions and then related to the local fluid structure via planar radial distribution functions. We find that local fluid properties correlate with the inhomogeneous fluid density and the strength of the wall-fluid interaction. Finally, we discuss the utility of this analysis in the interpretation of experiments involving the characterization of confined fluids.

DOI: 10.1103/PhysRevE.86.062501 PACS number(s): 78.55.Bq, 62.10.+s, 05.20.Jj

I. INTRODUCTION

Calculations of the mechanical properties of bulk liquids have been of interest for some time as they provide a testbed for the machinery of the statistical mechanics of fluids, especially analytical approximations to correlation functions [1,2]. Motivated by the technological importance of microfluidic and nanofluidic systems, in recent years workers have sought to quantify the role of liquid-solid interactions on fluid structure [3] and associated mechanical and transport properties [4] in confined fluids. In the case of confined fluids, these studies have included assessments of the role of fluid structure on slip boundary conditions and the characterization of propagating modes parallel to confining walls [5].

The mechanical behavior of confined fluids has been of particular interest in recent years owing to the growing importance of micro-electromechanical systems. For example, Barisik and Beskok [6] have performed molecular dynamics studies to examine local stress and density variations within a static, nanoscale-confined fluid, while Keshavarzi *et al.* [7] derived an expression for the local pressure tensor in nanoslit pores. Eslami *et al.* [8] developed a methodology to study layering as a function of pressure in a confined Lennard-Jones fluid and water, while Hartkamp *et al.* examined the anisotropy of the local stress in simulations of Poiseuille flow [9].

While the aforementioned studies have elucidated the behavior of the stress in confined fluids, comparatively little attention has been paid to the local elastic properties of these systems. Some notable work in this area includes an experimental characterization of the viscoelastic response of molecular layers in confined water [10] and a calculation of the viscoelastic properties from a statistical-mechanical treatment of a simplified model system [11]. By contrast, in bulk fluids, the local elastic constants have been calculated in a Lennard-Jones fluid [12] and a binary hard-sphere fluid [2] and related to fluid structure via the radial distribution function. The situation in confined fluids is expected to be more complex as local density variations induced by confining walls alter the high-frequency elastic response, leading to inhomogeneous elastic behavior that depends on the strength of the fluid particle and wall interaction.

In this paper, Monte Carlo simulation is used to determine the local, wave-number-dependent, high-frequency elastic properties of a confined fluid and to examine their dependence on density. For simplicity, our system comprises two walls of Lennard-Jones atoms bounding a Lennard-Jones fluid. The elastic constants of the fluid are calculated from spatial correlations of a coarse-grained stress and then related to the local fluid structure via the local density and planar radial distribution functions.

II. LOCAL ELASTIC CONSTANTS

A. Background: Bulk fluid

The high-frequency, elastic properties of a bulk fluid can be obtained from static spatial correlations of the Fourier transform of the stress $\sigma_{\alpha\beta}(\vec{k})$ in equilibrium, where $\vec{k}$ is the wave vector. For example, Schofield derived expressions for the high-frequency, local elastic constants of a bulk fluid [13]. He defined the components of the fourth-rank elastic constant tensor $C_{\alpha\beta\mu\delta}(\vec{k})$ in reciprocal (i.e., $\vec{k}$) space from an assumed linear constitutive relation between the components of the stress rate and the strain rate.

Now, by correlating the stress rate with the strain rate and invoking the stationary property of correlation functions, one finds that the elastic constants for a homogeneous, isotropic liquid having a density ρ are given by the stress-stress correlation functions $C_{\alpha\beta\mu\delta}(\vec{k}) = \beta/N\ \langle\sigma_{\alpha\beta}(\vec{k})\sigma_{\mu\delta}(-\vec{k})\rangle$ [13,14], where the angle brackets denote an equilibrium average and β is the inverse temperature. These correlation functions may be evaluated in terms of the radial distribution function $g(r)$, or, alternatively may be calculated by employing an explicit representation of the stress tensor. For example, using Voigt notation, Schofield expressed $c_{11}(k)$ in terms of $g(r)$ for a system described by a pair potential $u(r)$, and this expression can be written to highlight the k dependence as

$$c_{11}(k) = \left(\frac{3}{\beta}\right) + 2\pi\rho\left[\int_0^\infty drr^3 g(r)u'(r)p(kr) + \int_0^\infty drr^4 g(r)u''(r)q(kr)\right], \tag{1}$$

where

$$p(kr) = \frac{4}{3k^2r^2} + \frac{4\cos(kr)}{k^4r^4} - \frac{4\sin(kr)}{k^5r^5},$$
$$q(kr) = \frac{2}{3k^2r^2} - \frac{4\cos(kr)}{k^4r^4} - \frac{2(k^2r^2-2)\sin(kr)}{k^5r^5}. \tag{2}$$

The values of the elastic constants in the long-wavelength limit follows from $\lim_{x\to 0} p(x) = 2/15$ and $\lim_{x\to 0} q(x) = 1/5$.

An alternative route to calculating the elastic constants follows from an explicit representation for the stress. For a collection of atoms, each having a mass m, and described by a pair potential $u(r)$, the stress components at $\vec{r}$ are given by [15,16]

$$\sigma_{\alpha\beta}(\vec{r}) = \sum_i \frac{p_{i\alpha}p_{i\beta}}{m}\delta(\vec{r}-\vec{R}_i) - \frac{1}{2}\sum_i\sum_{j\neq i}\frac{R_{ij\alpha}R_{ij\beta}}{R_{ij}}\left(\frac{\partial u}{\partial R_{ij}}\right) \times \int_0^1 d\lambda\ \delta(\vec{r}-\lambda\vec{R}_j-(1-\lambda)\vec{R}_i), \tag{3}$$

where $\vec{R}_i$ ($\vec{p}_i$) is the canonical coordinate (momentum) of atom i and $R_{ij} = |\vec{R}_j - \vec{R}_i|$. Upon Fourier transforming Eq. (3) and using the equations for stress correlations, one can then determine the nonlocal elastic constants.

B. Inhomogeneous fluid

Our aim here is to characterize the elastic properties of an inhomogeneous fluid that is bounded as described above. As this fluid will be translationally invariant in the x-y plane, we define elastic constants in terms of the two-dimensional Fourier transformation

$$C_{\alpha\beta\gamma\delta}(\vec{k}_\parallel,z,z') = \beta\int d^2r\int d^2r' \exp[i\vec{k}_\parallel\cdot(\vec{r}-\vec{r}\,')_\parallel] \times\langle\sigma_{\alpha\beta}(\vec{r})\sigma_{\gamma\delta}(\vec{r}\,')\rangle, \tag{4}$$

where the "parallel" subscript indicates that a vector is confined to the x-y plane. Thus,

$$C_{\alpha\beta\gamma\delta}(\vec{k}_\parallel,z,z') = \beta\langle\sigma_{\alpha\beta}(\vec{k}_\parallel,z)\sigma_{\gamma\delta}(-\vec{k}_\parallel,z')\rangle, \tag{5}$$

where

$$\sigma_{\alpha\beta}(\vec{k}_\parallel,z) = \sum_i\frac{p_{i\alpha}p_{i\beta}}{m}\exp(i\vec{k}_\parallel\cdot\vec{R}_{i\parallel})\delta(Z_i-z) - \frac{1}{2}\sum_i\sum_{j\neq i}\frac{R_{ij\alpha}R_{ij\beta}}{R_{ij}}\left(\frac{\partial u}{\partial R_{ij}}\right)\exp(i\vec{k}_\parallel\cdot\vec{R}_{i\parallel}) \times f(\vec{k}_\parallel,z,\vec{R}_i,\vec{R}_j) \tag{6}$$

and

$$f(\vec{k}_\parallel,z,\vec{R}_i,\vec{R}_j) = \int_0^1 d\lambda\exp[i\lambda\vec{k}_\parallel\cdot(\vec{R}_j-\vec{R}_i)_\parallel] \times\delta[z-\lambda Z_j-(1-\lambda)Z_i]. \tag{7}$$

Rather than computing the elastic constants directly from Eq. (5), it is more convenient for implementation to define coarse-grained elastic constants in terms of an averaged stress tensor. This is accomplished by first integrating the stress components over a slab from z_1 to z_2 ($z_2 > z_1$) such that

$$\bar{\sigma}_{\alpha\beta}(\vec{k}_\parallel,z_1,z_2) = \int_{z_1}^{z_2}dz\ \sigma_{\alpha\beta}(\vec{k}_\parallel,z) = \sum_i\frac{p_{i\alpha}p_{i\beta}}{m}\exp(i\vec{k}_\parallel\cdot\vec{R}_{i\parallel})h(Z_i) - \frac{1}{2}\sum_i\sum_{j\neq i}\frac{R_{ij\alpha}R_{ij\beta}}{R_{ij}}\left(\frac{\partial u}{\partial R_{ij}}\right)e^{i\vec{k}_\parallel\cdot\vec{R}_{i\parallel}} \times\frac{\exp[i\lambda_2\vec{k}_\parallel\cdot(\vec{R}_j-\vec{R}_i)_\parallel]-\exp[i\lambda_1\vec{k}_\parallel\cdot(\vec{R}_j-\vec{R}_i)_\parallel]}{i\vec{k}_\parallel\cdot(\vec{R}_j-\vec{R}_i)_\parallel}, \tag{8}$$

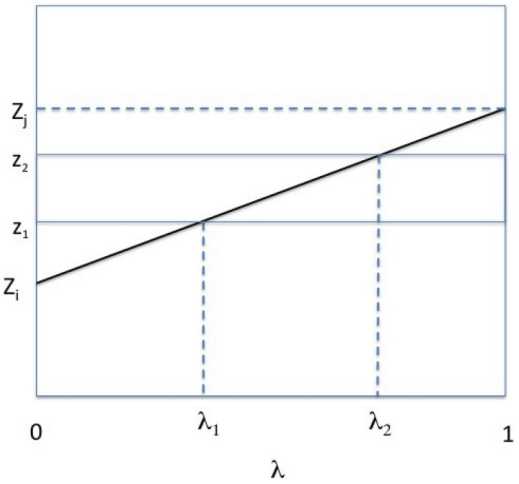

FIG. 1. (Color online) A graphical construction showing how to obtain the values λ_1 and λ_2 in Eq. (8). These values are determined by calculating the fraction of the line segment of length $Z_j - Z_i$ that lies within the averaging slab delimited by z_1 and z_2. The intercepts at $\lambda = 0$ and $\lambda = 1$ are Z_i and Z_j, respectively. For the example illustrated here, $\lambda_1 = (z_1 - Z_i)/(Z_j - Z_i)$ and $\lambda_2 = (z_2 - Z_i)/(Z_j - Z_i)$.

where

$$h(Z_i) = \Theta(Z_i - z_1)\Theta(z_2 - Z_i) \tag{9}$$

and where the values for λ_1 and λ_2 determine the fraction of the line joining points Z_i and Z_j that lies in the slab delimited by z_1 and z_2 (see Fig. 1). One can then define slab-averaged elastic constants using Eqs. (5) and (8) as

$$\bar{c}_{11}(k_\parallel) = \left(\frac{\beta}{N\Delta}\right)\langle\bar{\sigma}_{zz}(\vec{k}_\parallel)\bar{\sigma}_{zz}(-\vec{k}_\parallel)\rangle,$$
$$\bar{c}_{12}(k_\parallel) = \left(\frac{\beta}{N\Delta}\right)\langle\bar{\sigma}_{zz}(\vec{k}_\parallel)\bar{\sigma}_{xx}(-\vec{k}_\parallel)\rangle, \tag{10}$$
$$\bar{c}_{44}(k_\parallel) = \left(\frac{\beta}{N\Delta}\right)\langle\bar{\sigma}_{xy}(\vec{k}_\parallel)\bar{\sigma}_{xy}(-\vec{k}_\parallel)\rangle,$$

where $\Delta = z_2 - z_1$ and where, for convenience, the explicit dependence of quantities on z_1 and z_2 is not shown. We note that, in the presentation of results below, we focus on the configurational part of the elastic constants and, therefore, do not include trivial, kinetic (i.e., ideal gas) contributions.

III. SIMULATION PROCEDURE

Consider a monatomic fluid that is in a simulation cell with two confining walls, each normal to the z direction. The interactions between fluid atoms are described by a modified Lennard-Jones potential [17] with parameters ϵ and σ, and the wall-fluid interactions are described by a 9-3 Steele potential [18] that is obtained by assuming that the wall atoms are static and that they interact with fluid atoms via a standard Lennard-Jones potential (see the Appendix). For this interaction the relevant parameters are the wall density ρ_s and the potential parameters ϵ_s and σ_s. As usual, the length and energy scales are expressed in units of ϵ and σ, respectively. As will be seen below, the presence of the walls leads to spatial variations in the fluid density and, as a result, variations in the high-frequency elastic properties.

Conventional Metropolis Monte Carlo simulation is employed to take the system to equilibrium, starting from a face-centered cubic lattice, and to generate equilibrium configurations for the resulting fluid at constant temperature T. In addition to the stress correlations functions discussed above, the local average atomic number fraction $\langle\phi(z)\rangle$ (averaged over equilibrium configurations and the x-y plane) and the local, planar radial distribution function $g_{||}(r,z)$ (where r is the distance in the x-y plane) are calculated in equilibrium. The former quantity is calculated from a configurational average of the number of fluid atoms in a layer centered at z having a width δ. For these quantities, the label z denotes the center of an averaging slab in the z direction of width δ. For the radial distribution function, the normalizing density is calculated from the configurational average of the number of atoms in the planar region of interest divided by the planar area. As is customary, the results will be reported in reduced units.

In our simulations we employed a three-dimensionally periodic tetragonal cell having dimensions of $5a\times\ 5a\ \times\ La$, where $a = 1.564\sigma$, and containing N atoms at a reduced temperature T. Before simulating a confined fluid, for comparison we first model a bulk fluid having the same spatial average density ρ. For the case of a bulk fluid $L = 5$, whereas, for the case of a confined fluid, $L = 20$, but the fluid is confined between walls that are erected at $z = 0$ and $z = 10a$. Thus, in the latter case, the system consists of a confined fluid separated by walls. For the bulk fluid, we choose $N = 300$ ($\rho\sigma^3 = 0.627$) and $T = 1.13\epsilon/k_B$ such that the corresponding average pressure is nearly zero ($\langle P\rangle = 0.008\epsilon/\sigma^3$). For inhomogeneous fluids a system with $N = 600$ atoms at $T = 0.95\epsilon/k_B$ is confined to a region for which $L = 10$ (despite the larger cell) so that the *effective* density $\rho\sigma^3 = 0.627$. The density of the solid walls that confine the fluid is $\rho_s\sigma^3 = 1.045$. This temperature was selected so that the pressure when $\epsilon_s = 3.0$ is nearly zero. Typical runs consisted of 1.5×10^5 Monte Carlo steps (MCS), and the

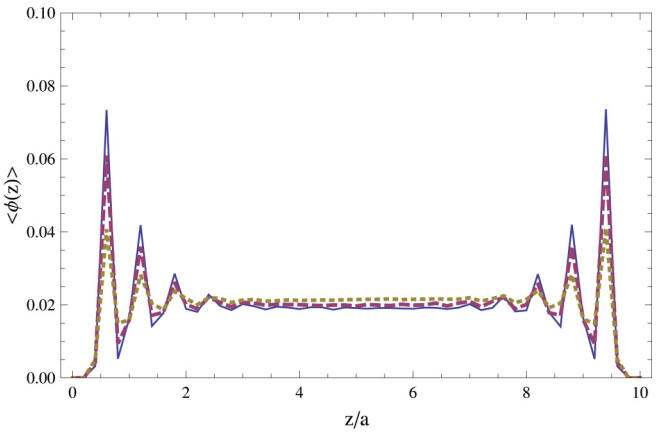

FIG. 2. (Color online) The local average atomic number fraction $\langle\phi(z)\rangle$ versus z/a, where $a = 1.564\sigma$, for a confined fluids with $\epsilon_s = 1$ (dotted line), $\epsilon_s = 2$ (dashed line), and $\epsilon_s = 3$ (solid line), respectively. The fluids are confined between walls located at $z = 0$ and $z = 10a$. In each case the average density $\rho\sigma^3 = 0.627$ and $T = 0.95\epsilon/k_B$. The width of the averaging slab $\delta = 0.2a$. Note the density oscillations induced by the wall.

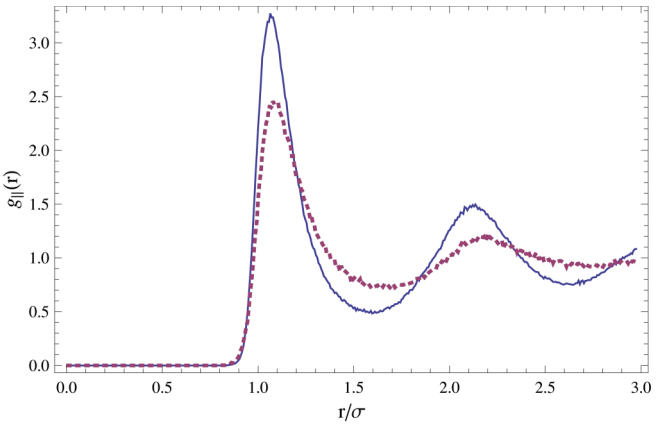

FIG. 3. (Color online) The local, planar radial distribution function $g_{||}(r)$ versus r/σ for $\epsilon_s = 1$ (dotted line) and $\epsilon_s = 3$ (solid line) for the region $z = 0.6a \pm \delta$. Note the larger height of the first peak for larger $\epsilon_s = 3$.

widths of the averaging slabs used for the inhomogeneous fluid are $\delta = 0.2a$ and $\Delta = 0.5a$. This value of Δ was chosen to be sufficiently large to average over many interatomic bonds, yet small enough to characterize local quantities. Several values of ϵ_s were used to model different fluid atom/wall interaction strengths.

IV. RESULTS

The presence of the walls induces a density variation in the fluid in equilibrium. This behavior is illustrated in Fig. 2 which shows the variation in the equilibrium fraction of fluid atoms $\langle\phi(z)\rangle$ as a function of z for several different values of ϵ_s for $\sigma_s = \sigma$ and average density $\rho\sigma^3 = 0.627$. It should be noted that the amplitude of the density oscillations decays relatively rapidly as a function of z, and that a fluid is locally denser for larger values of ϵ_s, as expected. Beyond these oscillations, system inhomogeneities also alter the local fluid structure and, therefore, the local elastic behavior. These changes in fluid structure are evident in the local, planar radial distribution

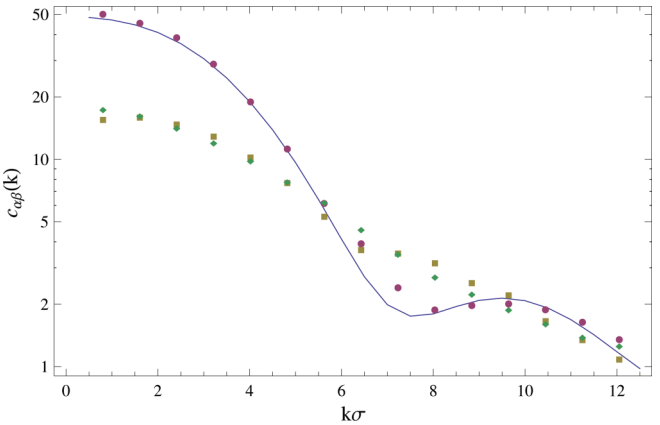

FIG. 4. (Color online) The elastic constants $c_{11}(k)$ (circle), $c_{12}(k)$ (square), and $c_{44}(k)$ (diamond) versus $k\sigma$ for the bulk fluid as determined from stress correlations. In addition, $c_{11}(k)$ is calculated from the radial distribution function [Eq. (1)] (solid line) to check the results.

function $g_{||}(r)$ near a wall, as shown in Fig. 3 for two values of ϵ_s. The increase in height of the first peak that attends an increase in ϵ_s reflects the additional near neighbors around an atom as the local density increases.

Before determining the elastic properties of the confined fluid, it is useful to examine the corresponding properties of the corresponding bulk fluid at the same average density and temperature. Figure 4 shows the dependence of $c_{11}(k)$, $c_{12}(k)$, and $c_{44}(k)$ on $k\sigma$ for the bulk fluid as determined from stress correlations. In addition, as a check, $c_{11}(k)$ is calculated from the radial distribution function [Eq. (1)]. The results imply that the fluid is more compressible at shorter wavelengths, where the compressibility $\kappa = 3/[c_{11}(k) + 2c_{12}(k)]$. Moreover, the fluid is only isotropic in the limit $k \to 0$ as the anisotropy parameter $c_{11}(k) - c_{12}(k) - 2c_{44}(k)$ only vanishes in this limit. Finally, we note that the oscillations in $c_{11}(k)$ occurring at large k can be traced to the oscillations in $h(kr)$.

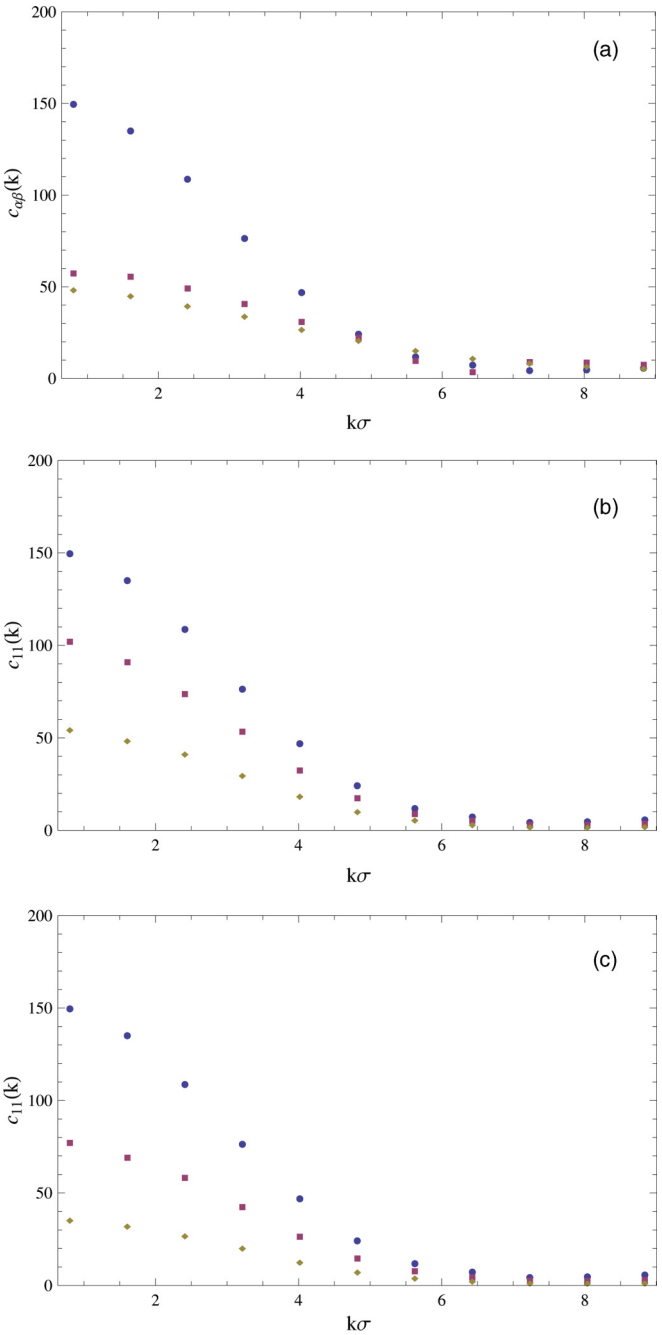

FIG. 5. (Color online) (a) The three nonlocal elastic constants $c_{11}(k)$ (circle), $c_{12}(k)$ (square), and $c_{44}(k)$ (diamond) versus $k\sigma$ for an inhomogeneous fluid near a wall ($0.5a \leqslant z \leqslant 1.0a$). For this case, $\epsilon_s = 3.0$. (b) The elastic constant $c_{11}(k)$ versus $k\sigma$ in the near-wall regime for three different values of ϵ_s, namely $\epsilon_s = 3.0$ (circle), $\epsilon_s = 2.0$ (square), and $\epsilon_s = 1.0$ (diamond). Clearly, this elastic constant is larger for larger values of ϵ_s. (c) The elastic constant $c_{11}(k)$ versus $k\sigma$ for $0.5a \leqslant z \leqslant 1.0a$ (circle), $1.0a \leqslant z \leqslant 1.5a$ (square), and $3.0a \leqslant z \leqslant 3.5a$ (diamond).

The three nonlocal elastic constants near a wall for the inhomogeneous fluid for $\epsilon_s = 3.0$ are shown in Fig. 5(a). As is evident upon comparison with Fig. 3, the fluid is "harder" for larger values of ϵ_s, presumably because $\langle\phi(z)\rangle$ is concomitantly larger in this regime (see Fig. 2). This trend is confirmed upon examining Fig. 5(b), which shows $c_{11}(k)$ as a function of $k\sigma$ in the same near-wall regime for three different values of ϵ_s. This elastic constant is larger for larger values of ϵ_s. Finally, Fig. 5(c) shows the variation of $c_{11}(k)$ with the distance from the wall z highlighting the decrease in this constant with decreasing fluid density.

V. CONCLUSION

We employed Monte Carlo simulation to calculate the local, wave-number-dependent (k), high-frequency elastic properties of a Lennard-Jones fluid that is confined between two walls. For this purpose, we constructed correlation functions of coarse-grained stresses in reciprocal space. It was found that local elastic properties correlate with the inhomogeneous fluid density and the strength of the wall-fluid interaction. Thus, we define position-dependent elastic constants whose values decay to their corresponding bulk values as one probes regions far from the walls. It is straightforward to employ this formalism for other confining geometries. Moreover, this analysis can be useful in the interpretation of laser trapping studies involving binary fluids [19] as these experiments probe the elastic response of fluids associated with depletion forces inherent in these systems [20].

APPENDIX

The wall-fluid potential can be obtained by considering a solid having density ρ_s forming two walls separated by a distance D. For the Lennard-Jones (i.e., 12-6) potential with energy parameter ϵ_s and length parameter σ_s, respectively, the resulting 9-3 potential is

$$U(z) = 4\pi\epsilon_s\rho_s\sigma_s^3\left\{\left[\frac{1}{45}\left(\frac{\sigma_s}{D-z}\right)^9 - \frac{1}{6}\left(\frac{\sigma_s}{D-z}\right)^3\right] + \left[\frac{1}{45}\left(\frac{\sigma_s}{z}\right)^9 - \frac{1}{6}\left(\frac{\sigma_s}{z}\right)^3\right]\right\}. \quad \text{(A1)}$$

The functional form of the modified Lennard-Jones potential $U_{BG}(r)$ due to Broughton and Gilmer [17] that we employ here is given in terms of the energy and length parameters ϵ and σ

by

$$U_{\mathrm{BG}}(r) = \begin{cases} 4\epsilon\left[\left(\frac{\sigma}{r}\right)^{12} - \left(\frac{\sigma}{r}\right)^{6}\right] + A_1, & r \leqslant 2.3\sigma, \\ A_2\left(\frac{\sigma}{r}\right)^{12} + A_3\left(\frac{\sigma}{r}\right)^{6} + A_4\left(\frac{r}{\sigma}\right)^{2} + A_5, & 2.3\sigma < r < 2.5\sigma, \\ 0, & r \geqslant 2.5\sigma, \end{cases} \tag{A2}$$

where $A_1 = 0.016\,132\epsilon$, $A_2 = 3136.6\epsilon$, $A_3 = -68.069\epsilon$, $A_4 = -0.083\,312\epsilon$, and $A_5 = 0.746\,89\epsilon$.

[1] R. Venkatesh and R. V. Gopala Rao, J. Phys. Chem. **98**, 9153 (1994).
[2] J. M. Rickman and H. D. Ou-Yang, Phys. Rev. E **84**, 012401 (2011).
[3] H. Abtahinia and F. Ebrahimi, J. Chem. Phys. **133**, 064502 (2010).
[4] N. Priezjev, in *Detection of Pathogens in Water*, edited by G. Zuccheri and N. Asproulis (IWA, London, 2012).
[5] F. Porcheron and M. Schoen, Phys. Rev. E **66**, 041205 (2002).
[6] M. Barisik and A. Beskok, Microfluid Nanofluid **11**, 269 (2011).
[7] T. Keshavarzi, F. Sedaghat, and G. A. Mansoori, Microfluid Nanofluid **8**, 97 (2010).
[8] H. Eslami, F. Mozaffari, J. Moghadasi, and F. Müller-Plathe, J. Chem. Phys. **129**, 194702 (2008).
[9] R. Hartkamp, A. Ghosh, T. Weinhart, and S. Luding, J. Chem. Phys. **137**, 044711 (2012).
[10] M. Antognozzi, A. D. L. Humphris, and M. J. Miles, Appl. Phys. Lett. **78**, 300 (2001).
[11] A. Würger, J. Phys.: Condens. Matter **23**, 505103 (2011).
[12] A. Z. Akcasu and F. Daniels, Phys. Rev. A **2**, 962 (1970).
[13] P. Schofield, Proc. Phys. Soc. **88**, 149 (1966).
[14] J. P. Boon and S. Yip, *Molecular Hydrodynamics* (Dover, New York, 1980).
[15] P. Schofield and J. R. Henderson, Proc. R. Soc. London A **379**, 231 (1982).
[16] Schofield and Henderson noted that the general expression for the stress tensor is given in terms of a contour integral that connects atomic positions [15]. This expression corresponds to the choice of a linear contour. For convenience, we do not introduce additional notation to distinguish between the stress in real space and reciprocal space.
[17] J. Q. Broughton and G. H. Gilmer, J. Chem. Phys. **70**, 5095 (1983).
[18] W. A. Steele, Surf. Sci. **36**, 317 (1973).
[19] J. Junio, S. Park, M.-W. Kim, and H. D. Ou-Yang, Solid State Commun. **150**, 1003 (2010).
[20] R. Castañeda Priego, A. Rodríguez-Lopéz, and J. M. Méndez-Alcaraz, J. Phys.: Condens. Matter **15**, S3393 (2003).